



LAWRENCE  
LIVERMORE  
NATIONAL  
LABORATORY

# Solvent Decomposition in Li-air Batteries: Impact of Peroxide and Superoxide Surface Terminations

N. Kumar, M. D. Radin, B. C. Wood, T. Ogitsu, K.  
Leung, D. J. Siegel

January 23, 2015

Journal of Physical Chemistry C

## **Disclaimer**

---

This document was prepared as an account of work sponsored by an agency of the United States government. Neither the United States government nor Lawrence Livermore National Security, LLC, nor any of their employees makes any warranty, expressed or implied, or assumes any legal liability or responsibility for the accuracy, completeness, or usefulness of any information, apparatus, product, or process disclosed, or represents that its use would not infringe privately owned rights. Reference herein to any specific commercial product, process, or service by trade name, trademark, manufacturer, or otherwise does not necessarily constitute or imply its endorsement, recommendation, or favoring by the United States government or Lawrence Livermore National Security, LLC. The views and opinions of authors expressed herein do not necessarily state or reflect those of the United States government or Lawrence Livermore National Security, LLC, and shall not be used for advertising or product endorsement purposes.

# Solvent Decomposition in Li-air Batteries: Impact of Peroxide and Superoxide Surface Terminations

Nitin Kumar<sup>a,b</sup>, Maxwell D. Radin<sup>c,†</sup>, Brandon C. Wood<sup>d</sup>, Tadashi Ogitsu<sup>d</sup>, Kevin Leung<sup>b</sup>, Donald J. Siegel<sup>a,c,\*</sup>

<sup>a</sup>Department of Mechanical Engineering, University of Michigan, Ann Arbor, MI 48109, USA

<sup>b</sup>Sandia National Laboratories, Albuquerque, New Mexico 87185, USA

<sup>c</sup>Department of Physics, University of Michigan, Ann Arbor, MI 48109, USA

<sup>d</sup>Lawrence Livermore National Laboratory, Livermore, California 94550

<sup>e</sup>Applied Physics Program, University of Michigan, Ann Arbor, MI 48109, USA

**KEYWORDS:** *Energy Storage; Surfaces and Interfaces; Electrolytes; Batteries; Density Functional Theory*

---

**ABSTRACT:** A viable Li/O<sub>2</sub> battery will require the development of stable electrolytes that do not continuously decompose during cell operation. Recent experiments suggest that reactions occurring at the interface between the liquid electrolyte and the solid lithium peroxide (Li<sub>2</sub>O<sub>2</sub>) discharge phase are a major contributor to these instabilities. To clarify the mechanisms associated with these reactions, a variety of atomistic simulation techniques – classical Monte Carlo, van der Waals-augmented density functional theory, *ab initio* molecular dynamics, and various solvation models – are used to study the initial decomposition of the common electrolyte solvent, dimethoxyethane (DME), on surfaces of Li<sub>2</sub>O<sub>2</sub>. Comparisons are made between the two predominant Li<sub>2</sub>O<sub>2</sub> surface charge states by calculating decomposition pathways on peroxide-terminated (O<sub>2</sub><sup>2-</sup>) and superoxide-terminated (O<sub>2</sub><sup>1-</sup>) facets. For both terminations DME decomposition proceeds exothermically via a two-step process comprised of hydrogen abstraction (H-abstraction) followed by nucleophilic attack. In the first step, abstracted H dissociates a surface O<sub>2</sub> dimer, and combines with a dissociated oxygen to form a hydroxide ion (OH<sup>-</sup>). The remaining surface oxygen then attacks the DME, resulting in a DME fragment that is strongly bound to the Li<sub>2</sub>O<sub>2</sub> surface. DME decomposition is predicted to be more exothermic on the peroxide facet; nevertheless, the rate of DME decomposition is faster on the superoxide termination. Finally, the impact of solvation (explicit *vs.* implicit) and an applied electric field on the reaction energetics are investigated. Our calculations shed light on the impact of surface charge state on electrolyte decomposition at liquid/solid interfaces in Li/O<sub>2</sub> batteries.

---

## INTRODUCTION

The high theoretical specific energy of the Li/O<sub>2</sub> battery<sup>1-6</sup> makes it a promising candidate for energy storage in electric vehicles (EVs). However, several performance gaps must be overcome for these systems to become commercially viable. One of the primary issues relates to decomposition of the organic electrolyte.<sup>7-18</sup> Decomposition processes have been associated with undesirable phenomena such as high charging overpotentials and limited cycle life.<sup>1,3,4,19,7,15,16,18</sup> Therefore, a deeper understanding of these reactions is an important step in developing practical Li/O<sub>2</sub> batteries.

Identifying a stable electrolyte for Li/O<sub>2</sub> batteries continues to be a challenge. Carbonates, a popular class of solvents for Li-ion batteries, appear to be incapable of providing<sup>7,9,10,12,14,15</sup> long cycle life and high round-trip efficiencies in these systems. For example, it has been shown that the primary discharge/charge reaction in a Li/O<sub>2</sub> battery using a carbonate-based electrolyte is not reversible formation/decomposition of Li<sub>2</sub>O<sub>2</sub>, but instead involves highly-stable phases such Li<sub>2</sub>CO<sub>3</sub> and/or other compounds which are generated by side reactions involving the electrolyte.<sup>7,9,14,15</sup>

More recent experiments have demonstrated an improvement with ether-based electrolytes, presumably due to their

higher stability with respect to decomposition during cell operation.<sup>3,6,13</sup> Despite this higher stability, several studies<sup>8,15,16,18,20</sup> have found evidence that side reactions persist in these systems. McCloskey *et al.*<sup>18</sup> quantified the yield of Li<sub>2</sub>O<sub>2</sub> in a Li/O<sub>2</sub> cell with a dimethoxyethane (DME) based electrolyte to be at best 91%. Based on the dependence of the Li<sub>2</sub>O<sub>2</sub> yield and columbic efficiency on discharge rate, it was concluded that the dominant parasitic reactions were chemical reactions between the Li<sub>2</sub>O<sub>2</sub> surfaces and the electrolyte. Specifically, the Li<sub>2</sub>O<sub>2</sub> yield increased with discharge rate while the columbic efficiency remained close to the ideal  $2 e^-/\text{O}_2$ , suggesting that shortening the exposure time of Li<sub>2</sub>O<sub>2</sub> surfaces to the electrolyte reduced the extent of side reactions. Freunberger *et al.* used FTIR, XRD and NMR to characterize discharged Li/O<sub>2</sub> batteries that used a tetraglyme-based electrolyte.<sup>8</sup> By the end of the first discharge cycle, decomposition products such as Li<sub>2</sub>CO<sub>3</sub>, HCO<sub>2</sub>Li, CH<sub>3</sub>CO<sub>2</sub>Li, polyethers, CO<sub>2</sub> and H<sub>2</sub>O were present (in addition to Li<sub>2</sub>O<sub>2</sub>). It was shown that changing either the salt, from LiPF<sub>6</sub> to LiTFSI, or the solvent, from tetraglyme to triglyme or diglyme, did not stop the formation of side products. Indeed, the accumulation of side reaction products has been suggested to contribute to poor voltaic efficiency and poor capacity retention.<sup>20,21</sup>

Bryantsev *et al.*<sup>22–24</sup> computationally screened a large number of solvents for reactivity with  $O_2$  and  $O_2^-$  species that may be present in  $Li/O_2$  batteries. It was suggested that the primary decomposition pathway of glymes was autooxidation to hydroperoxides and subsequent attack by  $O_2^-$ . In addition, Assary *et al.*<sup>25</sup> studied the decomposition of a representative ether solvent, DME, on  $Li_2O_2$  clusters<sup>26</sup>. It was found that DME preferred to decompose via H-abstraction on a Li-O-Li site that was suggested to be present as a defect or on small  $Li_2O_2$  nanoparticles. This defect oxide ( $O_2^-$ ) species was predicted to be more reactive than the peroxide ( $O_2^{2-}$ ) or superoxide ( $O_2^-$ ) species generally found on the low-energy  $Li_2O_2$  surfaces. Finally, Laino *et al.*<sup>27</sup> used first-principles metadynamics simulations to study the stability of various solvents in the presence of a peroxide terminated  $Li_2O_2$  surface. A long chain glyme, PEGDME, was proposed to be relatively stable.

These foregoing studies underscore the importance of understanding the mechanisms associated with electrolyte decomposition reactions. Revealing these mechanisms can suggest a rational pathway to developing electrolytes suitable for  $Li/O_2$  batteries. Towards this goal, the present study focuses on parasitic chemical reactions occurring at the  $Li_2O_2$ /electrolyte interface. Revealing these mechanism(s) remains a challenge due to the complex nature of the liquid electrolyte/solid electrode interface. For example, recent computational studies<sup>28</sup> have suggested that both peroxide and superoxide dimers can be present on  $Li_2O_2$  surfaces. Likewise, the impact of solvation by the electrolyte and the role of electric fields in the electrochemical double layer remain poorly understood. In principle all of these factors can impact the kinetics and thermodynamics of surface-mediated electrolyte decomposition.

The present study systematically explores these effects. More specifically, we examine DME decomposition atop low-energy peroxide and superoxide terminated  $Li_2O_2$  crystalline surfaces in order to discern the role of surface charge state on electrolyte decomposition. DME is predicted to decompose according to a two-step process on both surfaces; the first step involves H abstraction from DME and subsequent bonding to a surface  $O_2$  dimer. This interaction splits the dimer into an  $OH^-$  ion and an isolated O ion. In the second step, this residual O nucleophilically attacks the C site from which the H was abstracted, forming a strong bond between the broken DME and the surface. Regarding energetics, our calculations indicate that the decomposition reaction is more exothermic on the peroxide terminated surface; nevertheless, the activation energy for decomposition is lower on the superoxide surface, suggesting that this termination will be more reactive. Finally, the influence of solvation and electric fields on DME decomposition reactions is examined. An explicit solvation model generated from a snapshot of an *ab initio* MD simulation of a realistic electrolyte/ $Li_2O_2$  interface is compared with a continuum model and to a system where solvation effects are omitted. We find that the activation barriers are very similar across all three of these cases, suggesting that the energetics is dominated by short-ranged interactions. Effects due to an applied electric field are also discussed. This work clarifies the mechanisms associated with electrolyte decomposition in  $Li/O_2$  batteries and reveals the influence of surface charge state on those mechanisms.

## METHODOLOGY

Van der Waals (vdW) augmented DFT calculations were performed using the Vienna *ab initio* Simulation Package (VASP)<sup>29–31</sup>. The projector-augmented wave (PAW) scheme<sup>32,33</sup> was used to treat core-valence electron interactions, with the wave functions of the valence electrons expanded in a 400 eV plane wave basis set. All calculations were spin polarized. The PBE exchange-correlation functional<sup>34</sup> in conjunction with a fully self-consistent technique for treating dispersion interactions (optB88-vdW)<sup>35–37</sup> was the primary exchange correlation functional employed; additional spot-checking was performed using the HSE06 hybrid functional<sup>38,39</sup>.

Oxygen dimers on  $Li_2O_2$  surfaces were previously predicted to be electron-deficient in some low-energy terminations<sup>28</sup>. To isolate the role of the surface oxygen charge state on electrolyte decomposition, we selected two low-energy terminations that exhibit similar geometries but different charge states: the so-called (11-20) stoichi and the (11-20) O-rich-2 surfaces from Ref. 28. The oxygen dimers at the (11-20) stoichi surface are exclusively peroxides ( $O_2^{2-}$ ), whereas the oxygen dimers at the (11-20) O-rich-2 surface are exclusively superoxides ( $O_2^-$ ). Figure 1(a)-(b) depict these two surfaces. Additional information regarding these surfaces is provided elsewhere.<sup>28,40</sup>

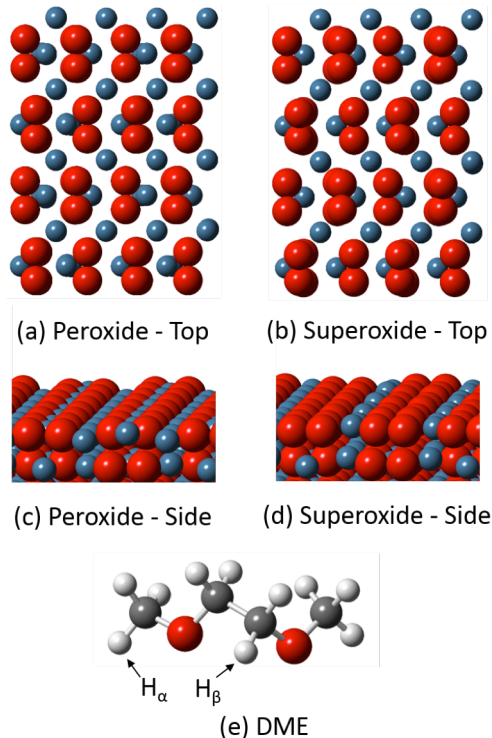


**Figure 1.** (a/c) and (b/d): Top/side view of the surfaces used for DME decomposition calculations. (a/c) peroxide-terminated (11-20) “stoichi” surface; (b/d) superoxide-terminated (11-20) “O-rich-2” surface; (e) Molecular structure of isolated DME with hydrogens labeled according to their location at primary  $CH_3-$  ( $H_\alpha$ ) and secondary  $-CH_2-$  ( $H_\beta$ ) carbon sites. The Li deficiency in the superoxide terminated  $Li_2O_2$  surface is visible in the side view (panel d) as missing Li ions within the  $O_2$  dimer rows. Li, O, C and H are shown with blue, red, grey and white, respectively.

The computational cell used for DME/Li<sub>2</sub>O<sub>2</sub> calculations consisted of a five-layer-thick Li<sub>2</sub>O<sub>2</sub> slab expanded 4 × 2 times in the surface plane, for a total of 160 atoms. The bottom three layers of the slabs were held fixed at their bulk positions; all other atoms were allowed to relax until the forces were less than 0.05 eV/Å. The dimensions of the simulation cell was 10.95 × 15.38 × 24 Å, which allows for the two surfaces of the Li<sub>2</sub>O<sub>2</sub> slab to be separated by 13.5 Å when the DME is adsorbed on the surface, ensuring minimal interaction between periodic images. As the molecule is placed only on one side of the slab, we examined the impact of dipole corrections and found that they had minimal effect (less than 0.02 eV) on the energetics. Hence, these corrections were not used in subsequent calculations.

Static and climbing-image nudged elastic band (NEB)<sup>41</sup> calculations were performed with Gamma point k-space sampling to estimate activation energies for DME decomposition reactions. Occasional spot check calculations were performed with higher k-point densities (2 × 2 × 1) and cut-off energies (550 eV). NEB barriers calculated using the denser k-point grid exhibit at most a ~0.01 eV increase in barrier height in comparison to the corresponding Gamma point calculation. The effect of increasing the plane-wave cut-off energy was also observed to be small: The DME adsorption energy increased by at most 8% at the 550 eV cutoff.

Starting configurations involving a single DME molecule adsorbed atop peroxide and superoxide terminated surfaces (Figure 2(a) and Figure 2(d)) were obtained using a two-step procedure. First, a classical Monte Carlo (MC) technique was used to sample the minimum energy configurations for DME adsorption on static Li<sub>2</sub>O<sub>2</sub> surfaces. The Universal Force Field (UFF) was used for these simulations,<sup>42</sup> with atomic partial charges determined by the Bader charge partitioning scheme.<sup>43-46</sup> More than 7000 conformations of DME were considered; these were generated by varying the torsion angles of the DME molecule. In addition, a large number of adsorption configurations (10<sup>7</sup>) were explored, using equal probabilities for rotation and translation with respect to the surface, and selection of different conformers.

In the second step of the procedure the 20 lowest energy configurations from the MC search were taken as starting configurations for geometry relaxations using vdW-DFT. Finally, the lowest energy DFT configurations were then used to study adsorption and decomposition energetics. A detailed search for low-energy DME configurations following H-abstraction was performed on the lowest energy DME adsorbed configuration on both peroxide and superoxide terminated Li<sub>2</sub>O<sub>2</sub> surfaces. In this case, the twelve hydrogens of the adsorbed DME were removed one by one and placed on various O<sub>2</sub> dimers on the surface. This process resulted in 70 configurations, from which the most stable H-abstracted configurations were selected as the most likely decomposition products. As described below, these products correspond to scenarios where the abstracted hydrogen resides on the O<sub>2</sub> dimer closest to the adsorbed DME.

The influence of an electric field normal to the surface plane was accounted for by including a charge dipole layer in the vacuum region at the simulation cell boundary.<sup>47,48</sup> The magnitude of the electric field was set to an average of 0.1 V/Å, which was selected to reproduce the expected potential drop for a typical electrochemical double layer. This value is obtained assuming a drop of ~1 V across a few nanometer

thick electric double layer atop the electrode. Other electric field strengths (0.01 and 0.001 V/Å) were also tested and found to have little impact on the reaction barrier.

The effects of solvation were included at two levels. First, a continuum solvation model (VASPsol code<sup>49-52</sup>) was used with the dielectric constant set to the value for DME ( $\epsilon = 7.2$ ).<sup>53</sup> Next an explicit model was explored by extracting a snapshot from an *ab initio* molecular dynamics (AIMD) run. This model was comprised of three regions: (i.) A four-layer thick Li<sub>2</sub>O<sub>2</sub> slab, constructed from a 3 × 2 supercell of the surface unit cell containing 168 atoms; (ii.) a liquid electrolyte containing 19 DME molecules and 2 LiBF<sub>4</sub> molecules, corresponding to a concentration of approximately 1 M; and (iii.) a ~14 Å vacuum region. The cell was orthorhombic, with dimensions 15.4 Å × 16.4 Å × 32.0 Å. The initial geometry was equilibrated for ~20 ps using the UFF<sup>42</sup> as implemented in GULP.<sup>54</sup> During this equilibration the Li<sub>2</sub>O<sub>2</sub> slab was held fixed. The system was then further equilibrated with AIMD using the QBox<sup>55,56</sup> code. These calculations were performed using the PBE GGA exchange correlation functional<sup>34</sup> with the D2 dispersion corrections of Grimme.<sup>57</sup> Gamma-point k-space integration was used. Norm-conserving HSCV pseudopotentials<sup>58</sup> were employed, with the hydrogen mass set to that of deuterium in order to improve time step convergence. The bottom layer of the Li<sub>2</sub>O<sub>2</sub> slab was kept fixed. A time step of 1 fs and temperature of 298 K was used for both classical and AIMD. Snapshots after ~20 ps of AIMD were extracted, relaxed to a local minimum, and subsequently used as starting points for NEB calculations. In addition, the energy barriers calculated using the NEB method were compared to a Metadynamics<sup>59-62</sup> simulation of the same. The simulation parameters for the Metadynamics run were identical to those used in the AIMD simulation. A Gaussian-shaped bias potential of 0.05 eV height and width was applied after every 25 fs of MD run-time to the bond connecting a  $\beta$ -hydrogen and C in the DME molecule.

## RESULTS

**Adsorption and decomposition of DME.** Figure 1 shows the peroxide (O<sub>2</sub><sup>2-</sup>) and superoxide (O<sub>2</sub><sup>-</sup>) terminated surfaces of Li<sub>2</sub>O<sub>2</sub> used for DME decomposition calculations. The DME molecule [Figure 1(c)] adsorbs exothermally on both surfaces [Figure 2(a) and Figure 2(d)]; we refer to these adsorbed geometries in which the DME does not spontaneously decompose as "intact" configurations. The calculated adsorption energies of an isolated DME molecule are -1.52 eV and -1.18 eV for the peroxide and superoxide terminated surfaces, respectively. The relaxed geometry suggests that there is a strong electrostatic interaction between the surface Li and ethereal (DME) O: on the peroxide surface, these Li-O distances are 2.04 Å and 2.10 Å, and on superoxide surface they are 2.03 Å and 2.02 Å. These bonds are slightly shorter than the Li-O bonds (2.16 Å) in the bulk peroxide.

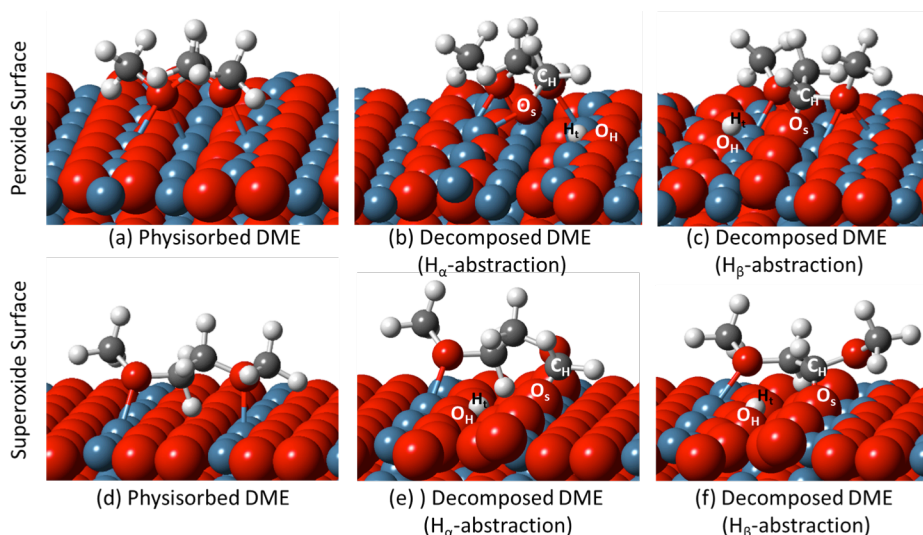


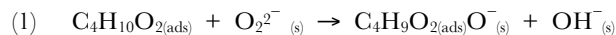
**Figure 2.** Side view of the low-energy configuration for adsorbed DME on peroxide (a) and superoxide surfaces (d). H-abstracted DME adsorbed atop peroxide (b,c) and superoxide surfaces (e,f). Abstracted H can detach from either  $-\text{CH}_3$  (a,c) or  $-\text{CH}_2-$  (b,d) positions within the adsorbed DME molecule. In all cases, H-abstraction results in splitting of an  $\text{O}_2$  dimer on the  $\text{Li}_2\text{O}_2$  surface, generating an  $-\text{OH}$  and a surface O that nucleophilically attacks the C from which H was abstracted.  $\text{H}_i$ : The H that is transferred from DME to the surface  $\text{O}_2$ .  $\text{C}_H$ : The C of DME from which  $\text{H}_i$  is abstracted.  $\text{O}_H$ : One of the surface O of  $\text{O}_2$  dimer that bonds with  $\text{H}_i$ .  $\text{O}_s$ : The other surface O of  $\text{O}_2$  dimer that nucleophilically attacks the  $\text{C}_H$ .

Potential decomposition pathways for adsorbed DME include C-O and C-H bond breaking reactions. The calculated activation barrier for C-O bond breaking was 2.5 and 1.7 eV for the superoxide and peroxide surfaces, respectively. These relatively high barriers suggest that DME decomposition is unlikely to proceed along such a pathway; hence, this mechanism was not considered further. A similar conclusion was also reported in a previous work.<sup>25</sup> On the other hand, decomposition of DME via an H-abstraction reaction was found to exhibit lower barriers on both types of  $\text{Li}_2\text{O}_2$  surfaces. In this case a hydrogen atom detaches from either the primary ( $\text{H}_\alpha$ ) or secondary ( $\text{H}_\beta$ ) position of DME (Figure 1(c)) and bonds to a surface  $\text{O}_2$  dimer. This process splits the  $\text{O}_2$  dimer resulting in the formation of a surface-bound hydroxyl (OH) species, and a residual, electron rich oxygen atom on the surface. This residual O then nucleophilically attacks the H-deficient C of the DME molecule. These two reactions, H-abstraction and nucleophilic attack, are roughly consecutive and result in highly exothermic products. Figure 2 illustrates the final configurations for decomposed DME fragments resulting from abstraction reactions involving  $\text{H}_\alpha$  or  $\text{H}_\beta$  on both surface terminations.

Figure 3 provides a summary of the thermodynamics and kinetics associated with the most favorable DME decomposition pathways for both surface terminations. The energies of the intact and decomposed states are given with respect to that of the separated components (an isolated DME molecule and the appropriate  $\text{Li}_2\text{O}_2$  surface). The activation energy for H-abstraction is given with respect to the intact configuration. It can be seen that the superoxide surface has a smaller (less exothermic) DME adsorption energy but lower activation energy for  $\text{H}_\beta$ -abstraction than the peroxide surface.

The overall decomposition reaction comprises an exchange of a hydrogen and an oxygen between the DME and surface

$\text{O}_2$  dimer. As shown by Bader analysis below, the net reaction on the peroxide terminated surface can be summarized as:



and that on the superoxide termination as:

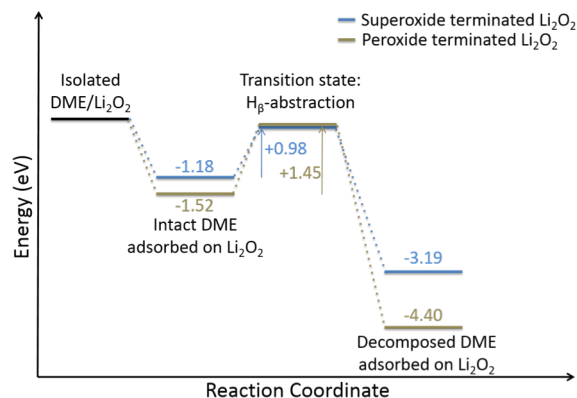
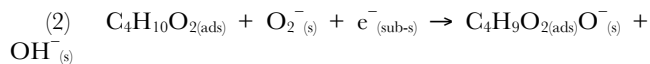


**Figure 3.** Energy landscape for  $\text{H}_\beta$ -abstraction from DME on peroxide and superoxide terminated  $\text{Li}_2\text{O}_2$  surfaces. ‘Isolated DME/ $\text{Li}_2\text{O}_2$ ’ refers to a configuration where DME and the  $\text{Li}_2\text{O}_2$  surface are separated. The activation barrier for H-abstraction is with respect to the ‘DME adsorbed on  $\text{Li}_2\text{O}_2$ ’ configuration, while the other energies are relative to the ‘Isolated DME/ $\text{Li}_2\text{O}_2$ ’ configuration.

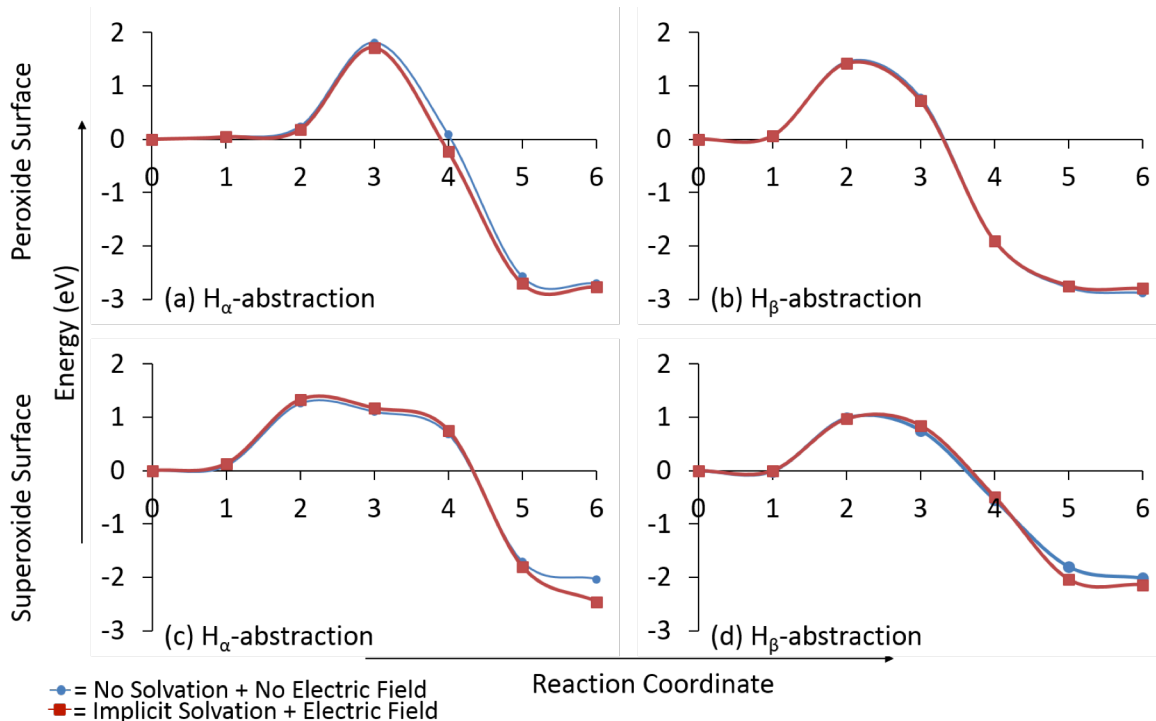


**Figure 4.** Energy profile for H-abstraction from DME adsorbed atop peroxide (a,b) and superoxide surfaces (c,d), computed at  $T = 0$  K using the NEB method with (■) or without (●) implicit solvation and electric field. In H-abstraction, H can detach from either  $-\text{CH}_3$  (a,c) or  $-\text{CH}_2-$  (b,d) position of the DME molecule. Image 0 corresponds to the intact configuration and Image 6 corresponds to the H-abtracted configuration for respective surfaces (Figure 2 shows these configurations). The 0 of y-axis correspond to the energy of the intact configuration.

Here,  $\text{C}_4\text{H}_{10}\text{O}_2(\text{ads})$  refers to the adsorbed (intact) DME, while  $\text{O}_2^{2-}(\text{s})$  and  $\text{O}_2^{\cdot-}(\text{s})$  are the peroxide and superoxide units on the respective surfaces that subsequently react with abstracted hydrogen. The product  $\text{C}_4\text{H}_{10}\text{O}_2(\text{ads})\text{O}^-(\text{s})$  species corresponds to H-abtracted DME bonded to a surface oxygen that is shared between DME and the surface; this species originates from the splitting of the  $\text{O}_2^{2-/1-}(\text{s})$  dimer due to interaction with abstracted H. Finally,  $\text{OH}^-(\text{s})$  represents the surface hydroxyl group formed from the dissociated  $\text{O}_2^{2-/1-}(\text{s})$  and abstracted H. In the latter case, as discussed below, one electron ( $e^-_{(\text{sub-s})}$ ) is transferred from peroxide moieties in the subsurface region of the slab.

For the peroxide surface, the products of reaction (1) are 2.70 and 2.88 eV lower in energy than the intact configuration when abstraction occurs at the  $\text{H}_\alpha$  and  $\text{H}_\beta$  sites, respectively. On the superoxide surface the products are 2.03 ( $\text{H}_\alpha$ ) and 2.01 eV ( $\text{H}_\beta$ ) lower in energy than the intact configuration. These energetics indicate that the thermodynamic driving force for DME decomposition is larger on the peroxide surface.

**Reaction barriers for DME decomposition.** The rate of the decomposition reaction is determined by the size of the reaction barrier(s) that must be surmounted to reach the reaction products. Figure 4 shows the reaction pathway for both  $\text{H}_\alpha$ - and  $\text{H}_\beta$ -abstraction from DME on the peroxide and superoxide terminated surfaces. The transition states for both abstraction sites correspond to a configuration where the abstracted H dissociates an  $\text{O}_2$  dimer forming an  $-\text{OH}$  and an electron rich O on the surface. The activation energies for these reactions on the peroxide surface are 1.81 and 1.45 eV

for the  $\text{H}_\alpha$  and  $\text{H}_\beta$ -abstraction, respectively. A similar trend with respect to the hydrogen sites is seen for the superoxide surface, where the reaction barriers are 1.26 and 0.98 eV for  $\text{H}_\alpha$  and  $\text{H}_\beta$ -abstraction, respectively. Taken together, these calculations suggest that abstraction of an  $\text{H}_\beta$  is more facile than abstraction of  $\text{H}_\alpha$ , independent of surface termination. In addition, the lower barrier found on superoxide terminated surfaces indicates that this termination is more reactive towards solvent decomposition than is the peroxide termination. The influence of using a hybrid functional (HSE06) on these two barriers was also examined by performing single point calculations on the relaxed energy pathway for  $\text{H}_\beta$ -abstraction. We find that the barrier increases consistently by 0.35 eV for both surfaces, but the trends observed between surface terminations or abstraction sites remain unchanged.

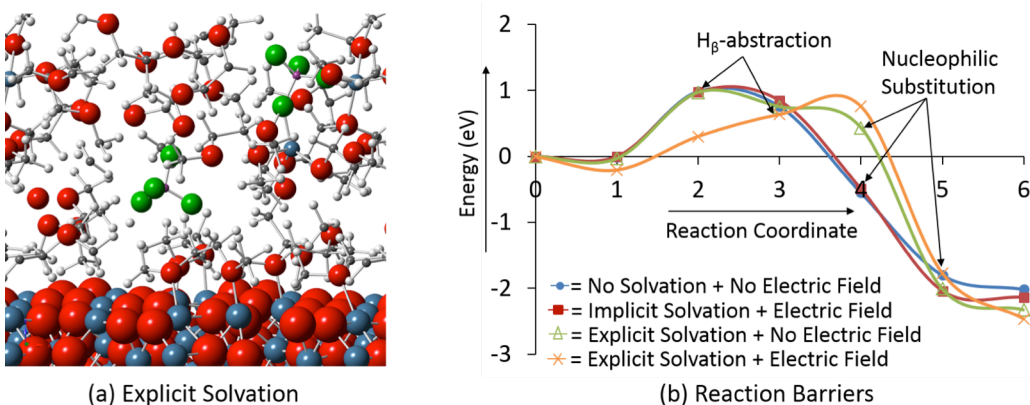


**Figure 5.** (a) A snapshot of an explicit electrolyte with 1 M  $\text{LiBF}_4$  salt/DME on the superoxide-terminated  $\text{Li}_2\text{O}_2$  surface. (b) Energy profile for  $\text{H}_\beta$ -abstraction from DME on the superoxide-terminated  $\text{Li}_2\text{O}_2$  surface, computed at  $T = 0$  K using the NEB method. The 0 of y-axis corresponds to the energy of the intact configuration. ‘ $\text{H}_\beta$ -abstraction’ and ‘Nucleophilic Substitution’ labels in (b) identify the mechanisms associated with the respective images in the NEB pathways. Li, O, C, H, B and F are shown in blue, red, grey, white, light pink and green, respectively.

**Effect of Solvation and Electric Fields.** The calculations described above are for an idealized case involving an isolated DME molecule adsorbed on a  $\text{Li}_2\text{O}_2$  surface. This may not be representative of the interface between the liquid electrolyte and a  $\text{Li}_2\text{O}_2$  surface in a  $\text{Li}/\text{O}_2$  cell due to the presence of salt/solvent molecules surrounding the DME undergoing H-abstraction, and also the presence of an electrochemical double layer that gives rise to an electric field in the vicinity of the interface due to charge separation.<sup>63</sup> In order to estimate the significance of these effects we have calculated abstraction barriers with a continuum solvation model and an electric field for hydrogen extraction from both sites ( $\text{H}_\alpha$  and  $\text{H}_\beta$ ) on both terminations (peroxide and superoxide). The magnitude and direction of electric field that most closely represents the environment of the  $\text{Li}_2\text{O}_2$ /electrolyte interface in a  $\text{Li}/\text{O}_2$  cell is unknown. We assume a nominal field magnitude of  $0.1 \text{ V}/\text{\AA}$ , motivated by the fact that electrochemical double layers typically exhibit potential drops on the order of a 1 V and thicknesses on the order of 1 nm.<sup>64</sup> We first consider the case where the field is oriented away from the surface, motivated by the predicted alignment of energy levels in  $\text{Li}_2\text{O}_2$  relative to the  $\text{Li}/\text{O}_2$  redox potential.<sup>65</sup>

We find that inclusion of implicit solvation and a  $0.1 \text{ V}/\text{\AA}$  electric field directed away from the surface has a small effect (at most  $\sim 0.1 \text{ eV}$ ) on the activation energy, as shown in Table 1 and Fig. 5. For example, the  $\text{H}_\beta$ -abstraction barrier decreases by only 0.02 and 0.01 eV for both peroxide and superoxide terminated surfaces, respectively. This effect is somewhat larger for the  $\text{H}_\alpha$ -abstraction where the barrier decreases by 0.09 eV on the peroxide and increases by 0.07 eV on the superoxide-terminated surfaces. Interestingly, when the direction of the electric field is reversed, *i.e.* pointing into the surface, the  $\text{H}_\beta$ -abstraction barrier on the superoxide-terminated surface is increased by a larger amount, from 0.97 to 1.33 eV.

The effect of solvation on the activation energy was further tested using a solvation model where both electrolyte and salt (1 M  $\text{LiBF}_4$ ) molecules are explicitly included. This was accomplished by extracting a representative configuration from large-scale *ab initio* MD, and then relaxing this configuration to a local energy minimum. While we believe that our starting structure for the explicit electrolyte case is well equilibrated, variations in the local electrolyte composition close to the DME – for example, a locally higher or lower concentration of salt ions – could in principle impact the barrier height. This

**Table 1** Energy barriers for H-abstraction from DME on the peroxide and superoxide terminated  $\text{Li}_2\text{O}_2$  surfaces as obtained from methods described in the text.

Site	Functional	Solvation	Electric field	Barrier: peroxide termination (eV)	Barrier: superoxide termination (eV)
$\text{H}_\alpha$	optB88-vdW	None	None	1.81	1.26
	optB88-vdW	Implicit	Away from surface	1.72	1.33
$\text{H}_\beta$	optB88-vdW	None	None	1.45	0.98
	optB88-vdW	Implicit	Away from surface	1.43	0.97
	optB88-vdW	Implicit	Towards surface	-	1.33
	optB88-vdW	Explicit	None	-	0.97
	optB88-vdW	Explicit	Away from surface	-	0.96
	HSE06 @ optB88-vdW	None	None	1.78	1.32

would be an interesting topic for additional investigation, but is beyond the scope of the present study. Due to the large computational cell used in these calculations, only the reaction with the lowest barrier from the isolated DME molecule calculations, *i.e.* H $\beta$ -abstraction on the superoxide terminated surface, was revisited in this scenario. We find that the size of the primary energy barrier obtained using the explicit solvation model is similar (0.97 eV) to that previously discussed for a single molecule (0.98 eV). The overall energy profile (Figure 5(b), green curve with triangular data points) is similar to the single molecule case, with the exception of the step where the surface O nucleophilically attacks the C of DME (image 4 in Figure 5(b)). This step is slightly less endothermic in the explicit electrolyte model, compared to the single molecule (blue curve, image 3 in Figure 5(b)), which can be explained by the fact that the neighboring electrolyte molecules may stabilize the H $\beta$ -abstracted DME, rendering it less susceptible to nucleophilic attack by the surface O. We also note that the DME fragment product resulting from the H $\beta$ -abstraction reaction (image 6 in Figure 5(b)) is more stable when it is coordinated by explicit electrolyte (-2.46 eV *vs.* the intact adsorbed DME) than in the single molecule case (-2.14 eV).

Additional quantification of the reaction barrier for H-abstraction was performed using a Metadynamics simulation. In this case the reaction barrier for H $\beta$ -abstraction was calculated to be  $1.04 \pm 0.01$  eV, in very good agreement with the NEB result.

The effect of an electric field (0.1 V/Å) on the explicitly modeled electrolyte was also tested (Figure 5(b), orange curve with ‘x’ data points). We find that the activation energy is reduced slightly to 0.96 eV, as can be seen by comparing image 4 (transition state) to image 1 (minimum energy configuration along the pathway). Interestingly, neither H $\beta$ -abstraction (image 3) nor nucleophilic attack (image 5) corresponds to the

**Table 2** Bader charges of the atoms participating in the decomposition reaction as a function of surface termination and H-abstraction site (alpha vs. beta).  $\Delta q$  corresponds to the change in charge with respect to the intact configuration;  $q$  corresponds to the absolute value of the charge on the various atoms. The labels H $\beta$ , O $\beta$ , O $\alpha$  and C $\alpha$  are shown in Figure 2.

Superoxide	$\Delta q$ slab	$\Delta q$ DME- H $\beta$	$q$ (O $\beta$ )	$q$ (H $\beta$ )	$q$ (O $\alpha$ )	$q$ (C $\alpha$ )
Intact	0.0	0.0	-0.5	0.1	-0.4	0.4
H $\beta$ - abstracted	-1.0	0.6	-1.3	0.6	-1.3	0.9
H $\alpha$ - abstracted	-1.1	0.6	-1.2	0.7	-1.5	0.9

Peroxide	$\Delta q$ slab	$\Delta q$ DME- H $\beta$	$q$ (O $\beta$ )	$q$ (H $\beta$ )	$q$ (O $\alpha$ )	$q$ (C $\alpha$ )
Intact	0.0	0.0	-0.8	0.1	-0.9	0.4
H $\beta$ - abstracted	-1.1	0.6	-1.3	0.6	-1.5	1.0

transition state in this case. Rather, the transition state occurs during the reorientation of the H $\beta$ -abstracted DME (approximately image 4) in preparation for nucleophilic attack. (In order to eliminate the lowering of energy for image 1 we repeated this barrier calculation with a relaxed version of image 1 as the starting configuration. But, the lowering of energy

persisted. This could be explained by the presence of local minima in other degrees of freedom within the electrolyte.)

Table 1 summarizes the decomposition energetics of DME under the various scenarios considered in this work. For a fixed direction of the applied electric field, the activation energy for the H-abstraction reaction is similar in all cases, regardless of whether an explicit electrolyte, with (0.97 eV) or without (0.96 eV) electric field, or a single molecule, with (0.97 eV) or without (0.98) solvation and electric field, is used. The similarity between reaction barriers obtained across the different models suggests that the key kinetic pathways for DME decomposition are largely determined by the local chemistry between the adsorbed DME molecule and the Li $_2$ O $_2$  surface, and are relatively insensitive to environmental effects.

**Charge transfer analysis.** A Bader charge analysis for the single DME molecule decomposition reaction shows that for both surface terminations a total of one electron ( $e^-$ ) is transferred from the DME to the Li $_2$ O $_2$  slab. Table 2 shows the charges on these atoms before and after reaction steps involving H-abstraction and nucleophilic attack on both surfaces. As expected, the pristine peroxide and superoxide terminated surfaces start with around 1 and 0.5  $e^-$  on each O, respectively. Roughly half an  $e^-$  is transferred when H $\beta$  is abstracted (comparing column 2 and column 3 of Table 2) and the other half is transferred after O $\beta$  nucleophilically attacks the C $\alpha$  (column 3 of Table 2). Interestingly, at the end of the reaction the O $\beta$  and O $\alpha$  have similar charge states on both surface terminations, although the peroxide O $_2$  dimers start with essentially twice the charge as found initially on the superoxide O $_2$  dimers. Since 1  $e^-$  is transferred to the Li $_2$ O $_2$  surface from the DME for both terminations, it would appear that there is some “unaccounted for” charge transferred to these atoms in the case of the superoxide termination. The source of the additional charge transferred to the superoxide surface can be identified by analyzing the charges on the neighboring O $_2$  dimers both along the surface and in the sub-surface region. Charge transfer from sub-surface peroxide moieties to the surface O $_2$  dimer that participates in the H-abstraction reaction was identified as the source of the additional transferred electrons.

**DME decomposition via alternative reaction routes.** Alternative reaction routes for H $\beta$ -abstraction of DME on the superoxide-terminated surface were also explored. Figure 6(a) shows one such reaction route that consists of three reaction steps. The first reaction is H $\beta$  transfer from DME to a surface O $_2$  where it forms a stable HOO $^-$  species on the surface, and the C $\alpha$  remains in a metastable sp $^2$  state. The barrier for this reaction is 1.09 eV. It is interesting to note that a stable OOH species can be observed on the superoxide-terminated surface. However, on the peroxide terminated surface, the presence of H $\beta$  near O $_2$  spontaneously splits the O $_2$  dimer. In the second step, H $\beta$  diffuses to a neighboring O $_2$ , again forming an HOO $^-$  moiety on the surface and leaving the previously attached O $_2$  intact. The barrier for this H-diffusion is high (1.48 eV). Finally, the O $_2$  nucleophilically attacks the C $\alpha$  in an exothermic reaction step. The reaction energy profile shows that this reaction route is limited by H-diffusion. The high barrier for H-diffusion encouraged us to look for other nucleophilic attack routes, such as the one shown in Figure 6(b). In this pathway, DME decomposition proceeds via two reaction steps. The first reaction is same as in the previous pathway: H $\beta$  is abstracted from the DME and subsequently bonds to a surface O $_2$ . The second step corresponds to a nu-

cleophilic attack by an  $O_2$  dimer that is located behind the DME molecule. The barrier for the second reaction is also high (1.36 eV). This high barrier could be due to the large distortion of DME that is needed to position the  $C_H$  in closer proximity to the surface  $O_2$  dimer that initiates the nucleophilic attack.

## DISCUSSION

A recent experiment<sup>18</sup> characterized the quantities of side reaction products formed in DME-based  $Li/O_2$  cells and found that the yield of  $Li_2O_2$  was at best  $\sim 90\%$ , thereby confirming the presence of (non- $Li_2O_2$  forming) parasitic reactions. Furthermore, Ref. 25 found evidence that the dominant solvent degradation mechanism during discharge was the chemical reaction between DME and  $Li_2O_2$  surfaces. The present calculations suggest that hydrogen abstraction from solvent molecules adsorbed on  $Li_2O_2$  surfaces may be the first step in this process.

To explore the hypothesis that chemical reactions between the solvent and  $Li_2O_2$  surfaces are responsible for the observed side reactions in  $Li/O_2$  cells, we use our predicted reaction barriers to estimate how much DME would be decomposed in a typical  $Li/O_2$  experiment. We assume that the reaction rate for solvent decomposition can be described by classical reaction theory; consequently, the number of moles of solvent that are decomposed per gram of cathode during a time  $t$  is given by  $N = c t A \nu \exp(-E_a/k_B T)$ , where  $A$  is the specific area of the discharge product,  $c$  is the concentration of active sites,  $\nu$  is a frequency factor, and  $E_a$  is the activation energy. Setting  $A = 100 \text{ m}^2/\text{g}_{\text{carbon}}$  (typical for carbon blacks<sup>66</sup>),  $c = 10^{19} \text{ m}^{-2}$  (based on the density of surface  $O_2$  sites),  $t = 6 \text{ h}$ ,  $\nu = 10^{13} \text{ Hz}$ <sup>25,67</sup>, and  $E_a = 1 \text{ eV}$  (our calculated reaction barrier) yields  $5 \times 10^{-3} \text{ mol}/\text{g}_{\text{carbon}}$ . (Using instead the HSE06 reaction barrier (1.32 eV) yields  $2 \times 10^{-8} \text{ mol}/\text{g}_{\text{carbon}}$ . These quantities represent rough estimates: assuming that the values of  $A$ ,  $c$ , and  $\nu$  are uncertain to within a factor of four, and that  $E_a$  can vary by  $\pm 0.1 \text{ eV}$ , then the amount of solvent degraded would exhibit an uncertainty of approximately two orders of magnitude.) Considering that the amount of  $Li_2O_2$  generated during a discharge to a capacity of  $1000 \text{ mAh}/\text{g}_{\text{carbon}}$  is  $2 \times 10^{-2} \text{ mol}/\text{g}_{\text{carbon}}$ , we conclude that the decomposition products generated via chemical reaction with  $Li_2O_2$  surfaces upon cycling could comprise a significant fraction of the discharge product and ultimately degrade cell performance. Furthermore, we note that the surfaces examined here do not contain defects of the type examined in prior computational studies<sup>25</sup>. If present in high enough concentrations, these defects could further accelerate the rate of electrolyte decomposition.

A few prior theoretical studies have also examined reactions between  $Li_2O_2$  and various solvents. A recent study used first-principles metadynamics to study the stability of common solvents on a  $Li_2O_2$  surface<sup>27</sup>. This study differs from ours in that: (i.) rather than DME, a long-chain glyme (PEGDME) was considered and (ii.) a different  $Li_2O_2$  surface was examined. Our prior calculations found that the surface used in Ref. 27 (which we refer to as 1-100 stoich-1) had a high surface energy of  $> 100 \text{ meV}/\text{\AA}^2$ ; in contrast, the surfaces used in the present work have surface energies of only 26 and 52  $\text{meV}/\text{\AA}^2$ .<sup>28</sup> Since surfaces having higher surface energies tend to be more reactive, one might expect that the decomposition reactions explored in Ref. 27 would exhibit lower activation energies. Nevertheless, despite the differences in chain length

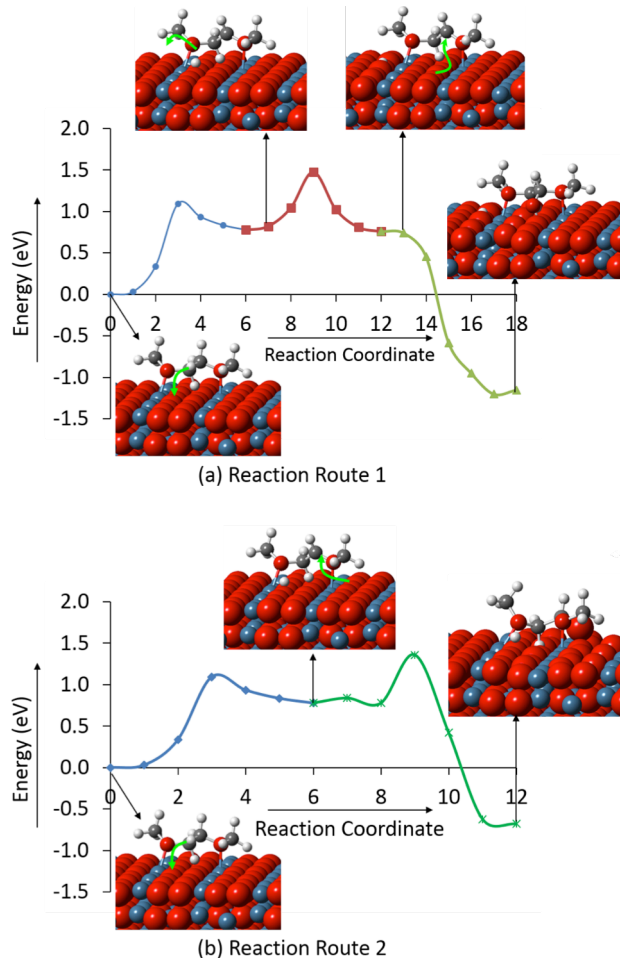


**Figure 6.** The energy profile for two reaction routes for DME decomposition on the superoxide surface, computed at  $T = 0 \text{ K}$  using the NEB method. The plots in different colors correspond to different parts of the reaction. The first part ( $\bullet$ ) of both reaction routes is an H-abstraction reaction where a stable OOH species is formed on the surface. This is followed by: (a) H-diffusion and  $O_2^{2-}$  nucleophilic attack on the H-abstrated C of DME or (b) direct nucleophilic attack by an oppositely placed  $O_2^{2-}$  dimer on the H-abstrated C of DME. The 0 of y-axis correspond to the energy of the intact configuration.

and surface termination, the results of Ref. 27 are largely consistent with ours: the decomposition of PEGDME was found to initiate with hydrogen abstraction, with a barrier of 0.90 eV at the PBE level of theory, and a barrier of 1.10 eV with the PBE0 hybrid functional.

In another computational study by Assary *et al.*<sup>25</sup> the decomposition of DME via H-abstraction was examined on cluster models of  $Li_2O_2$ , including the effects of a continuum model for solvation by an acetone solvent ( $\epsilon = 21$ ). It was found that DME decomposition was most favorable (0.66/1.01 eV activation energy using B3LYP/MP2, respectively) via  $H_\alpha$ -abstraction on a defective surface “Li-O-Li” site. Decomposition at peroxide and superoxide  $O_2$  moieties was found to yield higher barriers of 1.42/1.51 ( $H_\beta$ -abstraction) and 1.12/1.32 eV ( $H_\alpha$ -abstraction), respectively. The lower barriers observed for decomposition at superoxide sites is consistent with the

trends reported in the present study between superoxide and peroxide-terminated surfaces.

Bryantsev *et al.*<sup>22–24</sup> calculated the stability of DME with respect to reaction with solvated O<sub>2</sub> and O<sub>2</sub><sup>−</sup> molecules. Because of the large barrier for H<sub>α</sub>-abstraction by O<sub>2</sub><sup>−</sup> (~1.4 eV), it was concluded that hydrogen abstraction by superoxide species in solution was not competitive with disproportionation or electrochemical reduction. Our calculated H<sub>α</sub>-abstraction barrier of 1.26 eV on the superoxide surface is similar the B3LYP barrier calculated by Bryantsev *et al.*<sup>24</sup>

Alternatively, it was suggested<sup>22</sup> that decomposition of ether based electrolytes was due to autooxidation of DME in the presence of dissolved O<sub>2</sub>. The autooxidation process forms ether hydroperoxides that can then decompose in the presence of O<sub>2</sub>. How then does the rate of DME autooxidation compare to the rate of chemical attack of DME by Li<sub>2</sub>O<sub>2</sub> surfaces? As described above, this rate depends on the reaction barrier and the number of active surface sites or dissolved O<sub>2</sub> molecules. The reaction barrier for DME autooxidation calculated by Bryantsev *et al.*<sup>22</sup> (1.67 eV) is larger than the barriers for H-abstraction on Li<sub>2</sub>O<sub>2</sub> surfaces calculated in the present work. Additionally, the number density of surface dimers in a Li/O<sub>2</sub> cell during discharge will likely be larger than the number density of dissolved O<sub>2</sub> molecules: assuming similar properties to those described above (area of the discharge product = 100 m<sup>2</sup>/g<sub>carbon</sub>; density of surface sites = 10<sup>19</sup> m<sup>−2</sup>; density of the carbon electrode = 1 g<sub>carbon</sub>/cm<sup>3</sup>), we calculate a density of ~10<sup>3</sup> mol/m<sup>3</sup> of surface sites in the electrode. This is two orders of magnitude larger than the solubility of O<sub>2</sub> gas in DME: ~10/m<sup>3</sup>.<sup>68</sup> These data suggest that hydrogen abstraction at Li<sub>2</sub>O<sub>2</sub> surfaces likely dominates autooxidation during the discharge of Li/O<sub>2</sub> cells using DME-based electrolytes.

Comparing our results to prior calculations suggests two trends: the environment of a superoxide molecule (i.e., solvated, defective cluster, or clean surface) appears to influence the reaction barrier for H-abstraction from DME by a few tenths of an eV; and (2) the barriers for H abstraction from DME predicted by hybrid functionals tend to be a few tenths of an eV larger than those predicted by semilocal functionals. The later observation can be attributed to the enhanced localization of electrons typical of hybrid functionals, which may cause an increase to energy barriers for transition states that involve charge transfer.<sup>69</sup>

We emphasize that the barrier computed for DME solvated with explicit electrolyte approximates the electrolyte as a glassy solid rather than as true liquid. A similar approach has been used in other recent studies<sup>70–73</sup>. The validity of this approach is further supported by the fact that the reaction barrier for H<sub>β</sub>-abstraction calculated using Metadynamics (in combination with the explicit electrolyte) is nearly identical. It should be noted that the explicit electrolyte model includes different physics than the model based on implicit solvation: The explicit case includes the effects of local chemical bonding between DME and the solvent. However, because it relies on locally relaxed solvent configurations rather than full dynamics, it largely omits dipolar or dielectric response, and likely underestimates the solvent reorganization. On the other hand, the implicit solvation model includes the liquid dielectric and electrostatic response, but neglects chemical bonding with the solvent. The fact that the reaction barriers are essentially identical for both models implies that the aforementioned effects (chemical bonding with solvent + dielec-

tric/electrostatic/reorganization response) are less important than the specific interaction between DME and the surface. In other words, in this case we can reasonably conclude that the collective solvent effects are relatively minor.

## SUMMARY

Electrolyte decomposition remains one of the primary obstacles to realizing efficient, high-capacity Li/O<sub>2</sub> batteries. The identification of mechanisms resulting in the irreversible reaction of the electrolyte with soluble and insoluble reaction products is a crucial step in engineering electrolytes suitable for long-term use in these systems. Towards this goal, the present study examines the initial decomposition reaction of the prototype electrolyte solvent, DME, using vdW-augmented DFT calculations combined with several other theoretical techniques.

We find that the dominant decomposition reaction of DME on Li<sub>2</sub>O<sub>2</sub> surfaces consists of an initial H-abstraction step wherein a secondary hydrogen (H<sub>β</sub>) detaches from DME and bonds to an O<sub>2</sub> dimer on the surface. The abstracted hydrogen dissociates the O<sub>2</sub> dimer, resulting in the formation of an –OH group and an electron rich O. This residual oxygen subsequently attacks the under-coordinated C<sub>H</sub> in the DME, resulting in a DME fragment strongly-bound to the Li<sub>2</sub>O<sub>2</sub> surface. Calculated activation energies reveal that it is easier to abstract H<sub>β</sub> than H<sub>α</sub> for both peroxide and superoxide terminations. Moreover, we find that barriers for H<sub>β</sub>-abstraction are smaller on superoxide terminated surfaces (0.97 eV) than on peroxide terminated surfaces (1.45 eV). The effects of an implicit solvation model and electric field on the DME decomposition were explored. An electric field (0.1 V/Å) pointing away from the surface decreases the H<sub>β</sub>-abstraction barrier at most by 0.02 eV. However, when the field direction is reversed, the H<sub>β</sub>-abstraction barrier increases from 0.97 to 1.33 eV. H<sub>β</sub>-abstraction was also studied using an explicit solvation model that includes coordination effects from a multi-component (salt + solvent) liquid electrolyte. The explicit model corroborates the results predicted by the continuum solvation approximation, as the barriers obtained by the two models are similar (0.97 eV). The presence of an electric field with explicit solvation reduces the barrier by a negligible amount. A Bader charge analysis shows a total of 1 e<sup>−</sup> transferred from DME to slab for both the peroxide to superoxide terminated Li<sub>2</sub>O<sub>2</sub> surfaces. Moreover, a charge transfer from bulk peroxide to the surface superoxide moieties is seen on the superoxide-terminated surface. Combination of our calculated activation energies with classical rate theory indicates that hydrogen abstraction at Li<sub>2</sub>O<sub>2</sub> surfaces could account for the degradation of ether solvents in Li/O<sub>2</sub> cells observed by experiments. These surface-mediated decomposition processes are expected to out-pace liquid-phase processes such as solvent autooxidation by dissolved O<sub>2</sub>. Our findings point to the need for surface engineering strategies that can chemically passivate reactive Li<sub>2</sub>O<sub>2</sub> surfaces, or to chemical modifications of the solvent that impede abstraction processes<sup>74</sup>.

## AUTHOR INFORMATION

### Corresponding Author

\* djsiege@umich.edu

### Present Addresses

## ACKNOWLEDGMENT

This work was supported by the U.S. Department of Energy's U.S.-China Clean Energy Research Center for Clean Vehicles (CERC-CVC), grant no. DE-PI0000012. BCW acknowledges support from the LLNL Laboratory Directed Research and Development Grant 12-ER-053. Computing support came from the LLNL Institutional Computing Grand Challenge program. Part of work was performed under the auspices of the U.S. Department of Energy by LLNL under Contract DE-AC52-07NA27344. The authors also thank Dr. Erik Draeger for his assistance with QBox.

## REFERENCES

- (1) Abraham, K. M.; Jiang, Z. A Polymer Electrolyte-Based Rechargeable Lithium/Oxygen Battery. *J. Electrochem. Soc.* **1996**, *143*, 1–5.
- (2) Read, J. Characterization of the Lithium/Oxygen Organic Electrolyte Battery. *J. Electrochem. Soc.* **2002**, *149*, A1190–A1195.
- (3) Read, J. Ether-Based Electrolytes for the Lithium/Oxygen Organic Electrolyte Battery. *J. Electrochem. Soc.* **2006**, *153*, A96–A100.
- (4) Ogasawara, T.; Débart, A.; Holzapfel, M.; Novák, P.; Bruce, P. G. Rechargeable Li<sub>2</sub>O<sub>2</sub> Electrode for Lithium Batteries. *J. Am. Chem. Soc.* **2006**, *128*, 1390–1393.
- (5) Bruce, P. G.; Freunberger, S. A.; Hardwick, L. J.; Tarascon, J.-M. Li-O<sub>2</sub> and Li-S Batteries with High Energy Storage. *Nat. Mater.* **2012**, *11*, 19–29.
- (6) Jung, H.-G.; Hassoun, J.; Park, J.-B.; Sun, Y.-K.; Scrosati, B. An Improved High-Performance Lithium–air Battery. *Nat. Chem.* **2012**, *4*, 579–585.
- (7) Mizuno, F.; Nakanishi, S.; Kotani, Y.; Yokoishi, S.; Iba, H. Rechargeable Li-Air Batteries with Carbonate-Based Liquid Electrolytes. *Electrochemistry* **2010**, *78*, 403–405.
- (8) Freunberger, S. A.; Chen, Y.; Drewett, N. E.; Hardwick, L. J.; Bardé, F.; Bruce, P. G. The Lithium–Oxygen Battery with Ether-Based Electrolytes. *Angew. Chem. Int. Ed.* **2011**, *50*, 8609–8613.
- (9) Freunberger, S. A.; Chen, Y.; Peng, Z.; Griffin, J. M.; Hardwick, L. J.; Bardé, F.; Novák, P.; Bruce, P. G. Reactions in the Rechargeable Lithium–O<sub>2</sub> Battery with Alkyl Carbonate Electrolytes. *J. Am. Chem. Soc.* **2011**, *133*, 8040–8047.
- (10) Bryantsev, V. S.; Blanco, M. Computational Study of the Mechanisms of Superoxide-Induced Decomposition of Organic Carbonate-Based Electrolytes. *J. Phys. Chem. Lett.* **2011**, *2*, 379–383.
- (11) McCloskey, B. D.; Scheffler, R.; Speidel, A.; Bethune, D. S.; Shelby, R. M.; Luntz, A. C. On the Efficacy of Electrocatalysis in Nonaqueous Li–O<sub>2</sub> Batteries. *J. Am. Chem. Soc.* **2011**, *133*, 18038–18041.
- (12) Zhang, Z.; Lu, J.; Assary, R. S.; Du, P.; Wang, H.-H.; Sun, Y.-K.; Qin, Y.; Lau, K. C.; Greeley, J.; Redfern, P. C.; et al. Increased Stability Toward Oxygen Reduction Products for Lithium–Air Batteries with Oligoether-Functionalized Silane Electrolytes. *J. Phys. Chem. C* **2011**, *115*, 25535–25542.
- (13) Black, R.; Oh, S. H.; Lee, J.-H.; Yim, T.; Adams, B.; Nazar, L. F. Screening for Superoxide Reactivity in Li–O<sub>2</sub> Batteries: Effect on Li<sub>2</sub>O<sub>2</sub>/LiOH Crystallization. *J. Am. Chem. Soc.* **2012**, *134*, 2902–2905.
- (14) Veith, G. M.; Dudney, N. J.; Howe, J.; Nanda, J. Spectroscopic Characterization of Solid Discharge Products in Li–Air Cells with Aprotic Carbonate Electrolytes. *J. Phys. Chem. C* **2011**, *115*, 14325–14333.
- (15) McCloskey, B. D.; Bethune, D. S.; Shelby, R. M.; Girishkumar, G.; Luntz, A. C. Solvents' Critical Role in Nonaqueous Lithium–Oxygen Battery Electrochemistry. *J. Phys. Chem. Lett.* **2011**, *2*, 1161–1166.
- (16) McCloskey, B. D.; Speidel, A.; Scheffler, R.; Miller, D. C.; Viswanathan, V.; Hummelshøj, J. S.; Nørskov, J. K.; Luntz, A. C. Twin Problems of Interfacial Carbonate Formation in Nonaqueous Li–O<sub>2</sub> Batteries. *J. Phys. Chem. Lett.* **2012**, *3*, 997–1001.
- (17) Wang, H.; Xie, K. Investigation of Oxygen Reduction Chemistry in Ether and Carbonate Based Electrolytes for Li–O<sub>2</sub> Batteries. *Electrochimica Acta* **2012**, *64*, 29–34.
- (18) McCloskey, B. D.; Valery, A.; Luntz, A. C.; Gowda, S. R.; Wallraff, G. M.; Garcia, J. M.; Mori, T.; Krupp, L. E. Combining Accurate O<sub>2</sub> and Li<sub>2</sub>O<sub>2</sub> Assays to Separate Discharge and Charge Stability Limitations in Nonaqueous Li–O<sub>2</sub> Batteries. *J. Phys. Chem. Lett.* **2013**, *4*, 2989–2993.
- (19) Girishkumar, G.; McCloskey, B.; Luntz, A. C.; Swanson, S.; Wilcke, W. Lithium–Air Battery: Promise and Challenges. *J. Phys. Chem. Lett.* **2010**, *1*, 2193–2203.
- (20) McCloskey, B. D.; Bethune, D. S.; Shelby, R. M.; Mori, T.; Scheffler, R.; Speidel, A.; Sherwood, M.; Luntz, A. C. Limitations in Rechargeability of Li–O<sub>2</sub> Batteries and Possible Origins. *J. Phys. Chem. Lett.* **2012**, *3*, 3043–3047.
- (21) Shui, J.-L.; Wang, H.-H.; Liu, D.-J. Degradation and Revival of Li–O<sub>2</sub> Battery Cathode. *Electrochem. Commun.* **2013**, *34*, 45–47.
- (22) Bryantsev, V. S.; Faglioni, F. Predicting Autoxidation Stability of Ether- and Amide-Based Electrolyte Solvents for Li–Air Batteries. *J. Phys. Chem. A* **2012**, *116*, 7128–7138.
- (23) Bryantsev, V. S.; Giordani, V.; Walker, W.; Blanco, M.; Zecevic, S.; Sasaki, K.; Uddin, J.; Addison, D.; Chase, G. V. Predicting Solvent Stability in Aprotic Electrolyte Li–Air Batteries: Nucleophilic Substitution by the Superoxide Anion Radical (O<sub>2</sub><sup>•−</sup>). *J. Phys. Chem. A* **2011**, *115*, 12399–12409.
- (24) Bryantsev, V. S.; Uddin, J.; Giordani, V.; Walker, W.; Addison, D.; Chase, G. V. The Identification of Stable Solvents for Nonaqueous Rechargeable Li–Air Batteries. *J. Electrochem. Soc.* **2013**, *160*, A160–A171.
- (25) Assary, R. S.; Lau, K. C.; Amine, K.; Sun, Y.-K.; Curtiss, L. A. Interactions of Dimethoxy Ethane with Li<sub>2</sub>O<sub>2</sub> Clusters and Likely Decomposition Mechanisms for Li–O<sub>2</sub> Batteries. *J. Phys. Chem. C* **2013**, *117*, 8041–8049.
- (26) Lau, K. C.; Assary, R. S.; Redfern, P.; Greeley, J.; Curtiss, L. A. Electronic Structure of Lithium Peroxide Clusters and Relevance to Lithium–Air Batteries. *J. Phys. Chem. C* **2012**, *116*, 23890–23896.
- (27) Laino, T.; Curioni, A. Chemical Reactivity of Aprotic Electrolytes on a Solid Li<sub>2</sub>O<sub>2</sub> Surface: Screening Solvents for Li–air Batteries. *New J. Phys.* **2013**, *15*, 095009.
- (28) Radin, M. D.; Rodriguez, J. F.; Tian, F.; Siegel, D. J. Lithium Peroxide Surfaces Are Metallic, While Lithium Oxide Surfaces Are Not. *J. Am. Chem. Soc.* **2012**, *134*, 1093–1103.
- (29) Kresse, G.; Furthmüller, J. Efficient Iterative Schemes for Ab Initio Total-Energy Calculations Using a Plane-Wave Basis Set. *Phys. Rev. B* **1996**, *54*, 11169–11169.
- (30) Kresse, G.; Furthmüller, J. Efficiency of Ab-Initio Total Energy Calculations for Metals and Semiconductors Using a Plane-Wave Basis Set. *Comput Mater Sci* **1996**, *6*, 15–50.
- (31) Paier, J.; Marsman, M.; Kresse, G. Why Does the B3LYP Hybrid Functional Fail for Metals? *J. Chem. Phys.* **2007**, *127*, 024103–024103–10.
- (32) Kresse, G.; Joubert, D. From Ultrasoft Pseudopotentials to the Projector Augmented-Wave Method. *Phys. Rev. B* **1999**, *59*, 1758.
- (33) Blöchl, P. E. Projector Augmented-Wave Method. *Phys Rev B* **1994**, *50*, 17953.
- (34) Perdew, J. P.; Burke, K.; Ernzerhof, M. Generalized Gradient Approximation Made Simple. *Phys. Rev. Lett.* **1997**, *78*, 1396–1396.
- (35) Klimeš, J.; Bowler, D. R.; Michaelides, A. Chemical Accuracy for the van Der Waals Density Functional. *J. Phys. Condens. Matter* **2010**, *22*, 022201.
- (36) Klimeš, J.; Bowler, D. R.; Michaelides, A. Van Der Waals Density Functionals Applied to Solids. *Phys. Rev. B* **2011**, *83*, 195131.
- (37) Dion, M.; Rydberg, H.; Schröder, E.; Langreth, D. C.; Lundqvist, B. I. Van Der Waals Density Functional for General Geometries. *Phys. Rev. Lett.* **2004**, *92*, 246401.

- (38) Heyd, J.; Scuseria, G. E.; Ernzerhof, M. Hybrid Functionals Based on a Screened Coulomb Potential. *J. Chem. Phys.* **2003**, *118*, 8207–8215.
- (39) Krukau, A. V.; Vydrov, O. A.; Izmaylov, A. F.; Scuseria, G. E. Influence of the Exchange Screening Parameter on the Performance of Screened Hybrid Functionals. *J. Chem. Phys.* **2006**, *125*, 224106.
- (40) Radin, M. D.; Tian, F.; Siegel, D. J. Electronic Structure of Li<sub>2</sub>O<sub>2</sub> {0001} Surfaces. *J. Mater. Sci.* **2012**, *47*, 7564–7570.
- (41) Henkelman, G.; Uberuaga, B. P.; Jónsson, H. A Climbing Image Nudged Elastic Band Method for Finding Saddle Points and Minimum Energy Paths. *J. Chem. Phys.* **2000**, *113*, 9901–9904.
- (42) Rappe, A. K.; Casewit, C. J.; Colwell, K. S.; Goddard, W. A.; Skiff, W. M. UFF, a Full Periodic Table Force Field for Molecular Mechanics and Molecular Dynamics Simulations. *J. Am. Chem. Soc.* **1992**, *114*, 10024–10035.
- (43) Bader, R. F. W. *Atoms in Molecules - A Quantum Theory*; Oxford University Press: Oxford, 1990.
- (44) Henkelman, G.; Arnaldsson, A.; Jónsson, H. A Fast and Robust Algorithm for Bader Decomposition of Charge Density. *Comput Mater Sci* **2006**, *36*, 354–360.
- (45) Sanville, E.; Kenny, S. D.; Smith, R.; Henkelman, G. Improved Grid-Based Algorithm for Bader Charge Allocation. *J Comput Chem* **2007**, *28*, 899–908.
- (46) Tang, W.; Sanville, E.; Henkelman, G. A Grid-Based Bader Analysis Algorithm without Lattice Bias. *J Phys Condens Matter* **2009**, *21*, 084204.
- (47) Feibelman, P. Surface-Diffusion Mechanism versus Electric Field: Pt/Pt(001). *Phys. Rev. B* **2001**, *64*.
- (48) Neugebauer, J.; Scheffler, M. Adsorbate-Substrate and Adsorbate-Adsorbate Interactions of Na and K Adlayers on Al(111). *Phys. Rev. B* **1992**, *46*, 16067–16080.
- (49) Mathew, K.; Sundararaman, R.; Letchworth-Weaver, K.; Arias, T. A.; Hennig, R. G. Implicit Solvation Model for Density-Functional Study of Nanocrystal Surfaces and Reaction Pathways. *J. Chem. Phys.* **2014**, *140*, 084106.
- (50) Petrosyan, S. A.; Rigos, A. A.; Arias, T. A. Joint Density-Functional Theory: Ab Initio Study of Cr<sub>2</sub>O<sub>3</sub> Surface Chemistry in Solution. *J. Phys. Chem. B* **2005**, *109*, 15436–15444.
- (51) Letchworth-Weaver, K.; Arias, T. A. Joint Density Functional Theory of the Electrode-Electrolyte Interface: Application to Fixed Electrode Potentials, Interfacial Capacitances, and Potentials of Zero Charge. *Phys. Rev. B* **2012**, *86*, 075140.
- (52) Gunceler, D.; Letchworth-Weaver, K.; Sundararaman, R.; Schwarz, K. A.; Arias, T. A. The Importance of Nonlinear Fluid Response in Joint Density-Functional Theory Studies of Battery Systems. *Model. Simul. Mater. Sci. Eng.* **2013**, *21*, 074005.
- (53) Xu, K. Nonaqueous Liquid Electrolytes for Lithium-Based Rechargeable Batteries. *Chem. Rev.* **2004**, *104*, 4303–4418.
- (54) Gale, J. D.; Rohl, A. L. The General Utility Lattice Program (GULP). *Mol Simulat* **2003**, *29*, 291–291.
- (55) Gygi, F.; Draeger, E. W.; Schulz, M.; De Supinski, B. R.; Gunnels, J. A.; Austel, V.; Sexton, J. C.; Franchetti, F.; Kral, S.; Ueberhuber, C. W. Large-Scale Electronic Structure Calculations of High-Z Metals on the BlueGene/L Platform. In *Proceedings of the 2006 ACM/IEEE conference on Supercomputing*; ACM, 2006; p. 45.
- (56) Gygi, F. Architecture of Qbox: A Scalable First-Principles Molecular Dynamics Code. *IBM J RES DEV* **2008**, *52*, 137.
- (57) Grimme, S. Semiempirical GGA-Type Density Functional Constructed with a Long-Range Dispersion Correction. *J Comput Chem* **2006**, *27*, 1787–1799.
- (58) Vanderbilt, D. Optimally Smooth Norm-Conserving Pseudopotentials. *Phys. Rev. B* **1985**, *32*, 8412–8415.
- (59) Laio, A.; Parrinello, M. Escaping Free-Energy Minima. *Proc. Natl. Acad. Sci.* **2002**, *99*, 12562–12566.
- (60) Laio, A.; Rodriguez-Fortea, A.; Gervasio, F. L.; Ceccarelli, M.; Parrinello, M. Assessing the Accuracy of Metadynamics†. *J. Phys. Chem. B* **2005**, *109*, 6714–6721.
- (61) Laio, A.; Gervasio, F. L. Metadynamics: A Method to Simulate Rare Events and Reconstruct the Free Energy in Biophysics, Chemistry and Material Science. *Rep. Prog. Phys.* **2008**, *71*, 126601.
- (62) Bucko, T. Ab Initio Calculations of Free-Energy Reaction Barriers. *J. Phys. Condens. Matter* **2008**, *20*, 064211.
- (63) Desai, S. K.; Neurock, M. First-Principles Study of the Role of Solvent in the Dissociation of Water over a Pt-Ru Alloy. *Phys. Rev. B* **2003**, *68*, 075420.
- (64) Newman, J.; Thomas-Alyea, K. E. *Electrochemical Systems*; John Wiley & Sons, 2004.
- (65) Radin, M. D.; Siegel, D. J. In Preparation.
- (66) Lu, Y.-C.; Kwabi, D. G.; Yao, K. P. C.; Harding, J. R.; Zhou, J.; Zuin, L.; Shao-Horn, Y. The Discharge Rate Capability of Rechargeable Li-O<sub>2</sub> Batteries. *Energy Environ. Sci.* **2011**, *4*, 2999–3007.
- (67) Sholl, D.; Steckel, J. A. *Density Functional Theory: A Practical Introduction*; John Wiley & Sons, Inc., 2009.
- (68) Hartmann, P.; Grübl, D.; Sommer, H.; Janek, J.; Bessler, W. G.; Adelhelm, P. Pressure Dynamics in Metal–Oxygen (Metal–Air) Batteries: A Case Study on Sodium Superoxide Cells. *J. Phys. Chem. C* **2014**, *118*, 1461–1471.
- (69) Cohen, A. J.; Mori-Sánchez, P.; Yang, W. Insights into Current Limitations of Density Functional Theory. *Science* **2008**, *321*, 792–794.
- (70) Yeh, K.-Y.; Janik, M. J. CHAPTER 3. Density Functional Theory Methods for Electrocatalysis. In *RSC Catalysis Series*; Asthagiri, A.; Janik, M. J., Eds.; Royal Society of Chemistry: Cambridge, 2013; pp. 116–156.
- (71) Shi, C.; O’Grady, C. P.; Peterson, A. A.; Hansen, H. A.; Nørskov, J. K. Modeling CO<sub>2</sub> Reduction on Pt(111). *Phys. Chem. Chem. Phys.* **2013**, *15*, 7114–7122.
- (72) Rossmeis, J.; Skúlason, E.; Björketun, M. E.; Tripkovic, V.; Nørskov, J. K. Modeling the Electrified Solid–liquid Interface. *Chem. Phys. Lett.* **2008**, *466*, 68–71.
- (73) Skúlason, E.; Karlberg, G. S.; Rossmeis, J.; Bligaard, T.; Greeley, J.; Jónsson, H.; Nørskov, J. K. Density Functional Theory Calculations for the Hydrogen Evolution Reaction in an Electrochemical Double Layer on the Pt(111) Electrode. *Phys. Chem. Chem. Phys.* **2007**, *9*, 3241–3250.
- (74) Adams, B. D.; Black, R.; Williams, Z.; Fernandes, R.; Cuisinier, M.; Berg, E. J.; Novak, P.; Murphy, G. K.; Nazar, L. F. Towards a Stable Organic Electrolyte for the Lithium Oxygen Battery. *Adv. Energy Mater.* **2014**.

---

TOC figure:

**Electrolyte Decomposition Rate**

